Phys. Status Solidi C 7, No. 3–4, 1000–1004 (2010) / DOI 10.1002/pssc.200982815

physica status solidi pss c
www.pss-c.com
current topics in solid state physics

Investigation of electric charge transport in conjugated polymer P3HT: PCBM solar cell with temperature dependent current and capacitance measurements

Peiqing Yu*[1], Denis Mencaraglia[1], Arouna Darga[1], Anne Migan[1], Roshanak Rabdbeh[2], Bernard Ratier[2], and André Moliton[2]

[1] Laboratoire de Génie Electrique de Paris, CNRS UMR 8507, SUPELEC, UPMC, Université Paris VI, Université Paris-Sud, 11 Rue Joliot Curie, Plateau de Moulon, 91192 Gif-Sur-Yvette Cedex, France
[2] Institut Carnot XLim, UMR 6172, CNRS, Université de Limoges, 123 Avenue Albert Thomas, 87060 Limoges Cedex, France

Received 1 August 2009, revised 13 November 2009, accepted 16 November 2009
Published online 22 February 2010

PACS 73.40.-c, 73.61.Ph, 84.60.Jt

* Corresponding author: e-mail peiqing.yu@lgep.supelec.fr, Phone: +33 1 69 85 16 44, Fax: +33 1 69 41 83 18, Web: www.lgep.supelec.fr

We investigated quantitatively the electronic transport properties of a bulk heterojunction polymer/fullerene solar cell, based on structure Glass/ITO/P3HT:PCBM/Al. The current-voltage I-V characteristics in the intermediate positive bias and temperature regime (0.2 V ≤ V ≤ 1.5 V, 180 K ≤ T ≤ 250 K) can be well fitted by a modified Poole-Frenkel PF detrapping model. Combining these results with the high frequency capacitance measurements, we could then derive independently the absorber thickness and its dielectric constant. At low temperature (80 K ≤T ≤ 170 K), the I-V data can be well accounted for with Space Charge Limited Current (SCLC) regimes. At intermediate positive bias (1V≤V≤2.3V), the current is dominated by the trapped space charges with an exponential traps distribution, while at high positive bias (2.5 V ≤ V ≤ 4 V), the space charges due to injected free carrier play an important role for the conduction. From the fits to the two different SCLC models, we could then extract the electrically active defects parameters controlling the transport. These parameters were confirmed by space charge capacitance spectroscopy.

© 2010 WILEY-VCH Verlag GmbH & Co. KGaA, Weinheim

1 Introduction

Polymeric bulk heterojuntion (PBHJ) photovoltaic (PV) cells have attracted a great deal of attention because of their low cost, light weight, and mechanical flexibility. To date, one of the highest efficiency polymer PV cells (~6%) have been fabricated with an interpenetrating network of regioregular poly (3-hexylthiophene), P3HT (p-type) [1], and the fullerene derivative [6, 6]-phenyl-C61 butyric acid methyl ester, PCBM (n-type) [2, 3].

The charge transport in organic materials is one of the key factors which determine the overall performance [4]. A good understanding of the transport properties may help us to optimize the devices and achieve a competitive performance. However there is not a single mechanism who can describe all cases for PBHJ cells. Influenced by several factors, such as, coulomb potential, carrier injection, space charges, they involve the injection dominated and bulk dominated mechanisms. Both mechanisms have been proposed as the rate limiting process in the current-voltage behaviour of polymers [5]: injection dominated mechanisms are tunnelling and thermionic emission; charge limited conduction was proposed to be due to an exponential traps distribution [5]. To go further, the electrical charges transport and their interaction with electrically active defects are investigated in this work with the temperature dependence of I-V characteristics in dark, and then, correlated with capacitance spectroscopy measurements.

2 Experimental

The cells were prepared in a simple sandwich structure on glass substrates pre-coated with indium-tin (ITO) as hole-injecting anode. Except the blend preparation and the substrates cleaning, all the processing steps are performed in glove box nitrogen atmosphere for the next fabrication process. On top of ITO, a P3HT: PCBM layer (~200 nm thick) was deposited by spin casting from a blended solution in a 30:24 weight ratio. Following an annealing process, the cell is completed by the evaporation deposition of

WILEY InterScience® DISCOVER SOMETHING GREAT

© 2010 WILEY-VCH Verlag GmbH & Co. KGaA, Weinheim

the Al cathode under reduced pressure. All the cells have a 25 mm^2 active area defined by the common part of the active layer and Al cathode. The electrical contact was taken with a solvent free silver-loaded electro-conductor epoxide resin annealed under atmospheric pressure.

For the temperature dependence of I-V characteristics and the capacitance spectroscopy technique, the cells were placed in a liquid nitrogen cryostat, which enables the temperature to range between 80 and 480 K under 10^{-4} mbar vacuum. The I-V characteristics were measured between -4 V and +4 V. For each given bias, the voltage was kept constant for 1s before the current measurement was taken with a 0.1 V bias increment. For the admittance spectroscopy, an Agilent 4294A impedance analyzer was used in the parallel RC equivalent circuit mode to measure the zero dc bias complex admittance in the frequency range from 40 Hz to 100 kHz. The amplitude of the alternative signal was fixed at 50 mV.

3 Results and discussions

The shape of the I-V curves leads us to consider two transport phenomena in terms of positive bias and temperature ranges: i) for (0.2 V-1.5 V) and (180 K-260 K), the results are well fitted with PF model, ii) for (1.6 V-4 V) and (80 K-170 K), they are well fitted with SCLC models. To indicate the goodness of the fits, the correlation coefficient R is displayed with the curve fit equation.

3.1 Dark current–voltage characteristics

3.1.1 Intermediate temperature (180 K-260 K) and low bias (0.2 V-1.5 V): Poole-Frenkel (PF)

In the classic PF detrapping model, the electrical conductivity is explained as a phenomenon due to ionization and represented by [6, 7]:

$$\sigma = \sigma_0 \exp\left[\left(\frac{\beta_{PF}}{kT}\right)F^{\frac{1}{2}}\right] = q\mu_f n_f \quad \text{with } \beta_{PF} = \sqrt{\frac{q^3}{\pi\varepsilon_0\varepsilon_r}} \tag{1}$$

where n_f is the density of free carriers and μ_f their mobility.

With Ohm law, J=σF (F=electrical field), the current density can be expressed as: $J=q.\mu_f.n_f.F$. Both μ_f and n_f usually increase with increasing electric field [8-13]. In practice, μ_f and n_f may be coupled [9, 11]. This effect can be described with a modified PF-like model presented by S.G.Chen *et al.* [9] for organic semiconductors. Assuming that F=V/d, where V is the applied electrical bias and d the thickness of the organic semiconductor, this model leads to the following expression of the current density:

$$J = J_0 \exp\left[A\left(\frac{V}{d}\right)^{\frac{1}{2}}\right] \quad \text{with} \begin{cases} J_0 = q\dfrac{V}{d}n_d\mu_0 \exp\left[\dfrac{-E_{aJ}}{kT}\right] \\ A = \dfrac{\eta}{kT} = \alpha + \dfrac{\beta_{PF}}{kT} \end{cases} \tag{2}$$

where: n_d=density of doping, E_{aJ}=current activation energy, and α comes from the free carriers and coupling field dependency.

The J-V characteristics are well described by this modified PF model (Eq. (2)) in this regime (Fig. 1). The

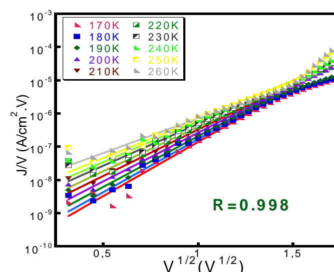

Figure 1 J-V characteristics in dark at medium temperature; experimental data (symbol), fit with PF model (full line).

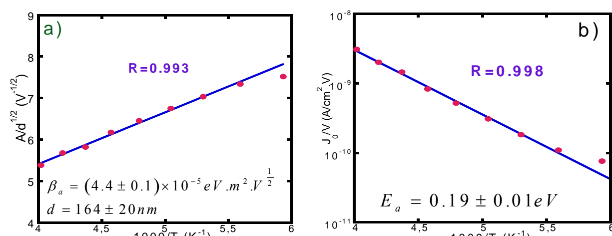

Figure 2 Temperature dependencies of parameters: a) $A/d^{1/2}$ and b) J_0/V extracted from the curves of Fig. 1 fitted with Eq. (2).

plots of $A/d^{1/2}$ and J_0/V versus 1/T are shown in Fig. 2. The expected $A/d^{1/2}$ is linear with 1/T. The activation energy of current density is extracted equal to 0.19±0.01 eV.

Combining the value of the slope of $A/d^{1/2}$ versus 1/T (Fig. 2(a)), with the dielectric capacitance derived from the high frequency capacitance measurement (Fig. 7), and taking into account the theoretical expression of β_{PF} (Eq. (1)), we could determine independently the thickness d and the relative dielectric constant ε_r of the P3HT: PCBM layer to be equal to 164±20 nm and 3.1±0.2 respectively, in good agreement with an independent mechanical measurement (for d) and the literature (for ε_r) [15]. Knowing these values is useful for the analysis of the other J-V regimes. With the fit of J_0/V versus 1/T, we could also derive the product $n_d\mu_0$ equal to 1.6×10^9 cm^{-1}.V^{-1}.s^{-1}.

3.1.2 Low temperature (80 K-180 K) and medium or high bias (1.6 V-4 V): SCLC

At low temperature, depending on the bias range, the J-V can be described with two types of SCLC mechanisms:

© 2010 WILEY-VCH Verlag GmbH & Co. KGaA, Weinheim

physica status solidi c

SCLC with an exponential traps distribution (SCLC-exp) and SCLC with field assisted mobility (SCLC-μ).

a. SCLC with exponential traps distribution (SCLC-exp):
The J-V characteristics presented in Fig. 3(a) in a log-log scale are analyzed using Eq. (3) representing the SCLC-exp model [14, 16-18]. A linear region can be seen for medium and high bias voltage, indicating that the J-V curves can be described with Eq. (3),

$$J = KV^{m} \text{ with } \begin{cases} m = l+1 = \dfrac{T_t}{T}+1 \\ K = \dfrac{q\mu N_{HOMO}}{d}\left(\dfrac{l}{l+1}\right)^{l}\left(\dfrac{2l+1}{l+1}\right)^{l+1}\left(\dfrac{\varepsilon}{qH_t d^2}\right)^{l} \end{cases} \quad (3)$$

where T_t represents the characteristic temperature of the exponential defect distribution and H_t is the integrated defect density in this distribution.

The temperature dependence of the exponent m is shown in Fig. 3(b). From this linear dependence, T_t = 479±6 K is extracted. This value was confirmed in our capacitance spectra study, which will be presented in the section 3.3. We note however on the equation of the linear fit (Fig. 4) that the ordinate axis intercept is closed to but not equal to 1, the expected theoretical value. We will come back later on this point.

b. SCLC with field-assisted mobility (SCLC- μ):
Figure 4 shows the J-V curves analyzed with SCLC-μ [17] for high bias values. In this model, with the presence of shallow traps of density n_t, Child's law remains valid with an effective mobility $\mu_{eff}=\theta\mu_f$ instead, where $\theta=n_f/(n_f+n_t)$ [16] depends consequently on temperature and field. In conjugated polymers, a field and temperature dependent mobility [5, 16, 17], measured by the TOF technique, has been successfully fitted by Gill [19]:

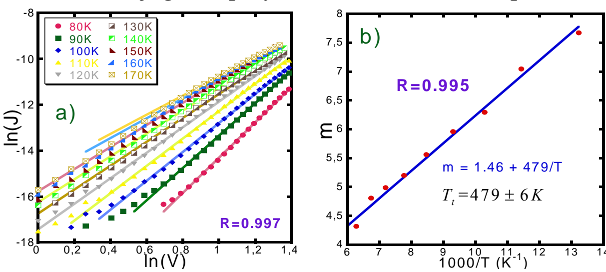

Figure 3 (a) J-V characteristics in dark at low temperature: experimental data (symbol), fit with SCLC-exp (full line); (b) exponent m versus 1/T for SCLC-exp.

$$\mu = \mu_0 \exp\left(-\frac{E_a}{kT}\right)\exp\left(\gamma\sqrt{F}\right), \quad \gamma = \frac{\beta}{kT_{eff}} \text{ with } \frac{1}{T_{eff}} = \frac{1}{T}-\frac{1}{T^0} \quad (4)$$

E_a is the trap depth [17], T^0 is a characteristic temperature [16, 19] and β is equal to β_{PF} or β_S ($=\beta_{PF}/2$) if the transport is bulk limited or controlled by a Schottky barrier at an interface respectively.

Then the current density can be expressed as:

$$J_{SCLC} = \frac{9}{8}\varepsilon\mu_{eff}\frac{V^2}{d^3} = J_0 \exp\left(\frac{\gamma}{d^{\frac{1}{2}}}V^{\frac{1}{2}}\right) \text{ with } \quad J_0 = \frac{9}{8}\varepsilon\mu_0\frac{1}{d^3}\exp\left(-\frac{E_a}{KT}\right) \quad (5)$$

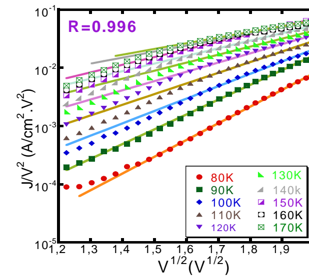

Figure 4 J-V characteristics in dark at low temperature: experimental data (symbol), fit with SCLC-μ model (full line).

Equation (5) was used to fit the data of Fig. 4 and the temperature dependencies of derived parameters $\gamma/d^{1/2}$ and J_0 are shown in Figs. 5(a) and (b) respectively, from which the factor β is determined to be the half of β_{PF}, derived in Section 3.1.1 (Fig. 2(a)), and E_a=0.13± 0.02 eV.

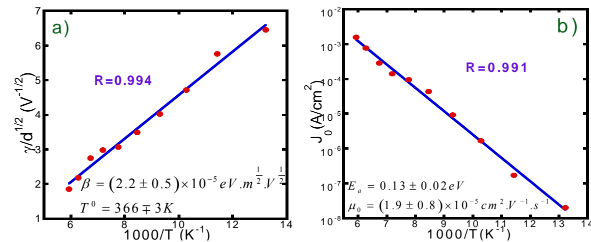

Figure 5 Temperature dependencies of parameters: a) $\gamma/d^{1/2}$ b) J_0 extracted from the curves of Fig. 5 fitted with Eq. (5).

3.2 Discussion for the two SCLC

Both SCLC models are in very good agreement with the experimental data. However, two questions are noticed: i) as mentioned above, for the exponent m, a small difference (≈0.5) is observed by comparing with the theoretical expression (Eq. (3)); ii) the two SCLC mechanisms used are dominated by different charges (due to traps or free carriers [5, 7]). To determine which SCLC model is the more appropriate, we will discuss them. We have also compared these two models with an extension of the SCLC-exp model adding to it the contribution of the free carriers to the space charge. We will call it SCLC2 (Fig. 6).

© 2010 WILEY-VCH Verlag GmbH & Co. KGaA, Weinheim

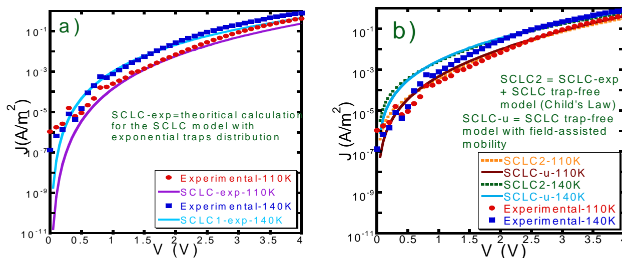

Figure 6 Experimental J(V) characteristics (symbols) and theoretical fits (full lines) with the different SCLC models.

Comparing these models with the experimental data (Fig. 6), we found that there is a threshold voltage about 2.3 V. Indeed, below 2.3 V, the model SCLC-exp is in good agreement with the experimental data (Fig. 6(a)) whereas for a larger bias, SCLC-μ and SCLC-2 give a better fit. Among these two last models, it is noteworthy that for both cases, the introduction of the free carriers contribution to the space charge makes the difference with the SCLC-exp model that cannot account satisfactorily for the experimental data for larger bias than 2.3 V.

This observation leads us to believe that the conduction is limited by the trapped space charges between 1 V and 2.3 V and then, from 2.3 V, not only the traps but also the injected free carriers play an important role in the SCLC model. The difference 0.5 observed for m is then attributed to the injected free carriers to the space charge.

3.3 Capacitance spectroscopy (C-F)

To confirm these results, the capacitance spectra C-F at zero dc bias was measured (Fig. 7). Using the model of Walter et al. [20], the inflexion point ω_t is given by:

$$\omega_t = T^2 \xi_0 . \exp\left(-\frac{E_a}{kT}\right) \tag{6}$$

where E_a represents the energetic level of the defect and the defect distribution is given by:

$$N_t(E) = -\frac{V_{bi}}{qkTw}\frac{d(C/S)}{d(\ln\omega)} \qquad E = kT\ln\left(\frac{2\nu_n}{\omega}\right) \tag{7}$$

where V_{bi} is the built-in potential fixed here to 0.93 V [21] and w the space-charge region width. Scaling the energy with the frequency using the pre-factor ξ_0 derived from the fit to Eq. (6), we plotted $N_t(E)$ for different temperatures (Fig. 7(b)). E_a also derived from the fit of Eq. (6) corresponds to the peak of the defect distribution (Fig. 7). The uncertainty of E_a comes mainly from the temperature measurements and the determination of ω_t. Considering them, we calculated E_a=0.14±0.01 eV.

We notice that part of this defect distribution can be well approximated with an exponential variation, having a characteristic energy of 42±6 meV (Fig. 7(b)). This value is close to the characteristic energy kT_t (41±1 meV) obtained from the SCLC-exp model (Section 3.1.2.(a)). A previous study leads us to think that such a defect could be related to intrinsic properties of the interpenetrated blend. Indeed we have shown that it still exists if a PEDOT: PSS layer is inserted between the ITO and organic blend, whereas another type of defect is eliminated with the buffer layer insertion [22]. Note that this second type of defect is also detected in the present investigated device having no PEDOT: PSS layer. Indeed this can be seen at low frequency on the C-F (Fig. 7(a)) where the drastic increase of the capacitance reveals the existence of this defect, however we could not quantitatively extract its parameters because it only begins to respond to the ac excitation in the investigated temperature and frequency ranges.

3.4 Comparison of extracted parameters

Table 1 Extracted parameters from PF model, two different SCLC models and capacitance spectra.

	PF	SCLC-exp	SCLC-μ	C (F,T)
T (K)	180-250	80-170	80-170	140-240
V (V)	0.2-1.5	1.6-3.5	2.6-4	-
μ_0 ($cm^2V^{-1}s^{-1}$)	(2.1±0.6) ×10^{-8}	(6.7±0.9)×10^{-8}	(1.9±0.8) ×10^{-5}	-
E_t (meV)	-	41±1	-	42±6
T_t(K)	-	479	-	486
$E_{a\text{-}defect}$ (eV)	-	-	0.13±0.02	0.14±0.01
$\beta_{PF/S}$ ($eVm^{1/2}V^{1/2}$)	β_{PF} (4.4±0.2)×10^{-5}	-	β_S (2.2±0.5)×10^{-5}	-

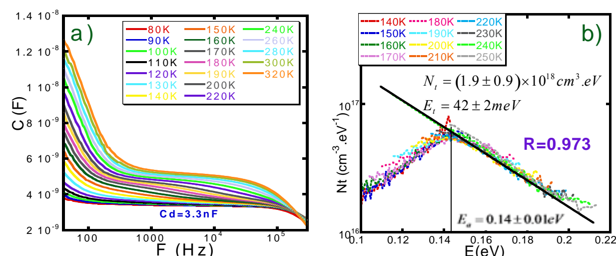

Figure 7 Capacitance spectra (a) and derived defect density (b).

For comparison, the different extracted parameters are gathered in Table 1. We can notice that: i) the zero-field mobility of PF and SCLC-exp model has the same order of magnitude: we suggest that it represents the conduction due to holes [18] and the one of SCLC-μ is due to the electrons injected from the Al contact, the contribution of which becomes more significant from 2.3 V, ii) the exponential part of the traps distribution is well confirmed by C-F with the same T_t value which was also obtained in our previous studies with the same materials but different geometry [22]; moreover, the peak defect depth of 0.14 eV is confirmed by SCLC-μ, iii) in SCLC-μ, $\beta=\beta_{PF}/2$, which suggests the existence of a Schottky barrier at the Al/P3HT: PCBM electron injecting contact. We propose that the derived density of localized states represents a hole trap distribution peaked at 0.14 eV from the HOMO level of p-type P3HT. The lowest mobility reported in Table 1 is controlled by this trap distribution. We cannot ascertain how-

© 2010 WILEY-VCH Verlag GmbH & Co. KGaA, Weinheim

ever that this can be ascribed to intrinsic properties of the blend as opposed to impurities, because as we mentioned above at the end of Section 3.3, another type of defect has also been detected, which was linked to the absence of PEDOT: PSS and probably related to the chemical reduction of ITO by the polymer blend. To what extent, this other non intrinsic defect could influence the presently derived mobility still disserves further investigation.

4 Conclusions

The present results demonstrated that the electrical transport in an ITO/P3HT: PCBM/Al heterostructure can be described with PF and SCLC conduction depending on the bias and temperature range. Analyzing and confirming with capacitance spectroscopy, we conclude that at intermediate temperature and low voltage, the transport is controlled by the coulomb potential in term of PF detrapping model and that holes are the predominant carriers. At low temperature, except at low bias, the conduction is limited by the space charge. This model is discussed with the nature of charge: at intermediate bias, the charges (holes) limiting the conduction are trapped in an exponential part of the localized states distribution, while at high bias, the space charge comes not only from the traps but also from the free carriers (electrons) injected at the Al/P3HT: PCBM interface acting as a Schottky contact.

Acknowledgements This work was partially founded under French ANR PV program (contact N° ANR-06-PSPV-003-05).

References

[1] T. A. Chen, R. D. Rieke, J. Am. Chem Soc. **114**, 10087 (1992).
[2] J. C. Hummelen, B.W. Knight, F. LePeq, F. Wudl, J. Yao, C. L. Wilkins, J. Org. Chem. **60**, 532 (1995).
[3] G. Dennler, M. C. Scharber, C. J. Brabec, Adv. Mater. **21**, 1-16 (2009).
[4] N. D. Nguyen, M. Schmeits, H.P.Lozbl, Phys. Rev. B **75**, 075307 (2007).
[5] A. J. Campbell, D. D. C. Bradley, D. G. Lidzey, J. Appl. Phys. **82**, 6326-6342 (1997).
[6] V. Dyakonov, D. Godovsky, J. Meyer, J. Parisi, Synth. Metals **124**, 103-105 (2001).
[7] Frenkel, J. Phys. Rev. **54**, 647 (1938).
[8] S. S. Sun, N. S. Sariciftci, Organic Photo Voltaic: Mechanisms, Materials, and Devices (Taylor & Francis, Boca Raton, 2005), chap. 6 (B. A. Gregg), pp. 16-18.
[9] S. G. Chen, P. Stradins, B. A. Gregg, J. Phys. Chem. B **109**, 28 (2005).
[10] B. A. Gregg, S. E. Gledhill, B. Scott, J. Appl. Phys. **99**, 116104 (2006).
[11] B. A. Gregg, J. Phys. Chem. B **108**, 17285 (2004).
[12] S. C. Jain, W. Geens, A. Mehra, V. Kumar, T. Aerons, J. Poortmans, R. Mertens, M. Willander, J. Appl. Phys. **89**, 3804 (2001).
[13] B. A. Gregg, S. G. Chen, H. M. Branz, Appl. Phys. Lett. **84**, 10 (2004).
[14] K. Kumari, S. Chand, P. Kumar, S. N. Sharma, V. D. Vankar, V. Kumar, Appl. Phys. Lett. **92**, 263504 (2008).
[15] G. Garcia-Belmonte, A. Munar, E. M. Barea, J. Bisquert, I. Ugarte, R. Pacios, Org. Electron. **9**, 847 (2008).
[16] K. C. Kao, W. Hwang, Electrical Transport in Solids (Pergamon Press, Beccles and London, 1981), chap. 3, p. 159.
[17] A. J. Campbell, M. S. Weaver, D. G. Lidzey, D. D. C. Bradley, J. Appl. Phys. **84**(12), 6737 (1998).
[18] C. Brabec, V. Dyakonov, J. Parisi, N. S. Sariciftci, Organic Photovoltaics: Concepts and Realization (Springer, Berlin 2003), chap. 5, pp. 172, 174.
[19] W. G. Gill, J. Appl. Phys. **43**, 12 (1972).
[20] T. Walter, R. Herberholz, C. Müller, H. W. Schock, J. Appl. Phys. **80**, 4411 (1976).
[21] L. Boeano, S. A. Carter, J. C. Scott, G. G. Malliaras, P.J. Brock, Appl. Phys. Lett. **74**, 1132 (1999).
[22] A. Migan-Dubois, D. Mencaraglia, P. Yu, Z. Djebbour, S. Bailly, N. Lemaître, R. De Bettignies, S. Guillerez, Journées annuelles de la SF2M 2008, Paris, France (2008).

© 2010 WILEY-VCH Verlag GmbH & Co. KGaA, Weinheim